

HYDROGEN BLENDING TO REDUCE CARBON EMISSIONS FROM THE METALS INDUSTRY

Joseph Smith[‡], Ahti Suo-Anttila[§], Vikram Sreedharan[‡], Zachary Smith[‡]

[‡]Chemical and Biochemical Engineering, Missouri Univ of Sci and Tech, Rolla, MO 65409 USA

[§]Computational Engineering Analysis LLC, 4729 Paso Del Puma Ne, Albuquerque, NM 87111 USA

[‡]Elevated Analytics Consulting, 343 East 4th Street, Suite 104, Rexburg, ID 83440 USA

ABSTRACT

Processing metals contributes significantly to carbon emissions (see Figure 1). This industry includes production facilities that smelt, refine, and cast ferrous and nonferrous metals including primary aluminum, ferroalloy, iron and steel, lead, magnesium, and zinc. These metals are produced from ore, pig, or scrap using electrometallurgical and other methods. Iron and steel are produced in foundries while primary aluminum, ferroalloy, lead, magnesium, and zinc are mainly produced in smelters or refineries for casting activities. Each of these production methods rely on stationary fuel combustion sources which traditionally rely on hydrocarbon fuels to generate the required heat. This industry therefore represents a significant opportunity for carbon emissions reduction by blending hydrogen with the hydrocarbon fuels.

2021 Total Reported Emissions from the Metals Sector, by Subsector

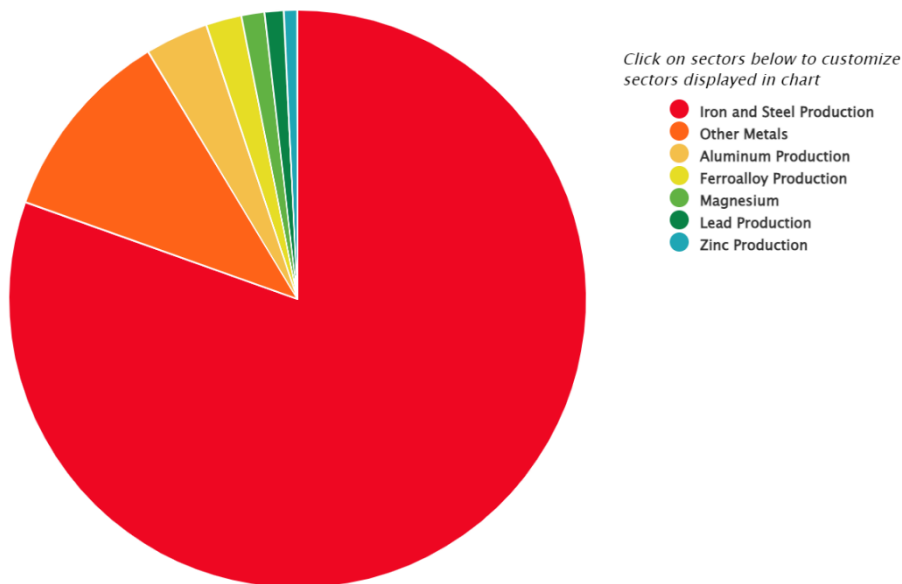


Figure 1 - 2021 Total Reported Direct Emissions from Metals, by Subsector (as of 8/12/2022)*

This paper discusses work using a transient multi-physics Computational Fluid Dynamics (CFD) model to simulate combustion of hydrocarbon fuels blended with hydrogen to reduce carbon emissions. The paper also discusses the impact of hydrogen blending on nitrogen oxide formation and other combustion emissions generated during the combustion process. The work

*see <https://www.epa.gov/ghgreporting/ghgrp-metals#trends-subsector>

demonstrates fuel blending to reduce carbon emissions to decarbonize metals production. The validated CFD model can also be used to optimize burner/furnace design that improves combustion efficiency and process safety when using hydrogen/hydrocarbon fuels. Predicted performance has been validated by direct comparison to measured data in burner tests.

INTRODUCTION AND OBJECTIVES

Many industrial applications burn hydrocarbon fuels to generate process heat required during the manufacturing process. One example of particular interest is the metals industry. In 2018, for each ton of steel produced, 1.85 tons of CO₂ was generated - about 8% of the global CO₂ emissions.¹ Globally, steel production must find ways to de-carbonize this industry to remain competitive in a “carbon-constrained” world economy. One focus of the steel industry is finding ways to use green hydrogen² in the direct reduction of iron ore using Electric Arc furnaces. This involves using hydrogen to decarbonize by replacing coal as a fuel in the process. The current work focuses on blending hydrogen with fossil fuels, i.e., hydrocarbon fuel such as natural gas (NG), propane (C3) or Liquid Petroleum Gas (LPG). The work discussed below examines using blended fuels in hybrid gas burners, such as the one depicted in Figure 2, in an industrial process such as the steel making process.

Another example where blended fuels can be used is in the petrochemical industry. Olefin production (see Figure 3) employees wall and floor burners (see Figure 4 and Figure 5) to generate high temperature surfaces inside various heater configurations (see Figure 6) where the hot walls and flames provide thermal radiation to heat process tubes where ethylene is cracked to produce poly-ethylene for plastics industry. Like the steel industry, olefins production also generates high levels of carbon emissions because hydrocarbon fuels including NG, C3, and LPG are burned. In general, any process that involves combustion, gasification or pyrolysis must either use carbon capture and sequestration (CCS) or carbon capture and utilization (CCU) to meet increasingly stringent carbon emissions requirements or use “non-carbon” or “low-carbon” fuels. Low-carbon fuels such as hydrogen/hydrocarbon blends can help industry reduce carbon emissions which can reduce or even eliminate the “capture” step and the associated costs of CCS/CCU.

¹ Christian Hoffmann, C., Van Hoey, M., Zeumer, B. “Decarbonization challenge for steel - Hydrogen as a solution in Europe,” McKinsey & Company (April 2020); see <https://www.mckinsey.com/industries/metals-and-mining/our-insights/decarbonization-challenge-for-steel#/>

² Hydrogen produced by electrolysis using electricity produced from renewable energy is termed “green hydrogen”. “Grey hydrogen” is defined as hydrogen produced from fossil fuels such as steam methane reforming while “Blue hydrogen” is defined as hydrogen produced from a process where CO₂ emissions are captured and either stored (CCS) or used (CCU).



Figure 2 - Multi-fuel burner with main fuel tips (purple) and blended fuel tips (green)

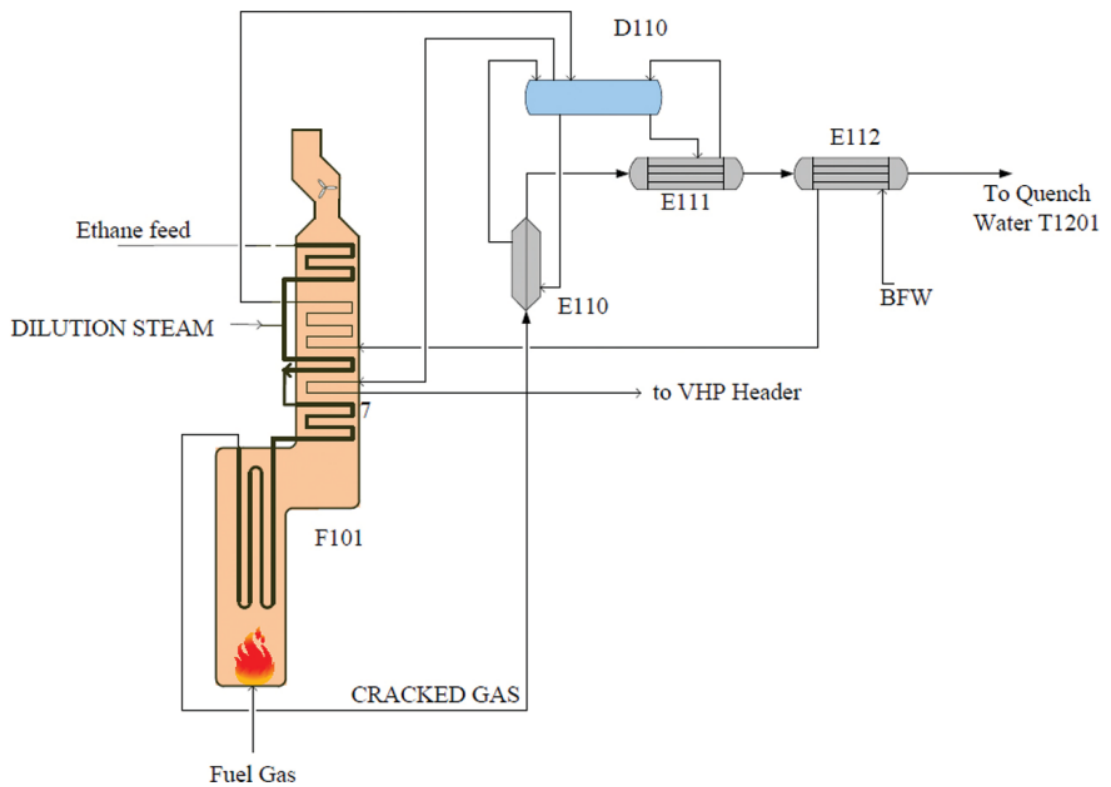


Figure 3 - Olefin production process showing fired section³

³ Barza, A., Mehri, B., Pirouzfard, V. (2018) "Mathematical Modeling of Ethane Cracking Furnace of Olefin Plant with Coke Formation Approach," *International Journal of Chemical Reactor Engineering*, 20170243; <http://doi.org/10.1515/ijcre-2017-0243>.

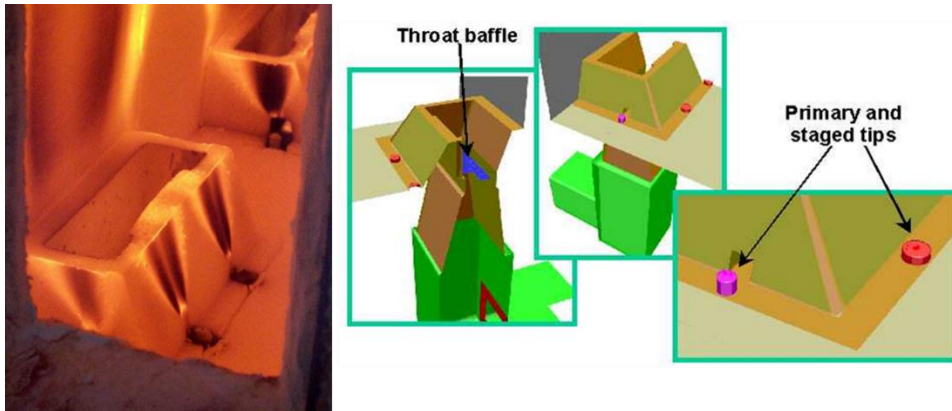


Figure 4 - Floor burner used in Olefin furnace

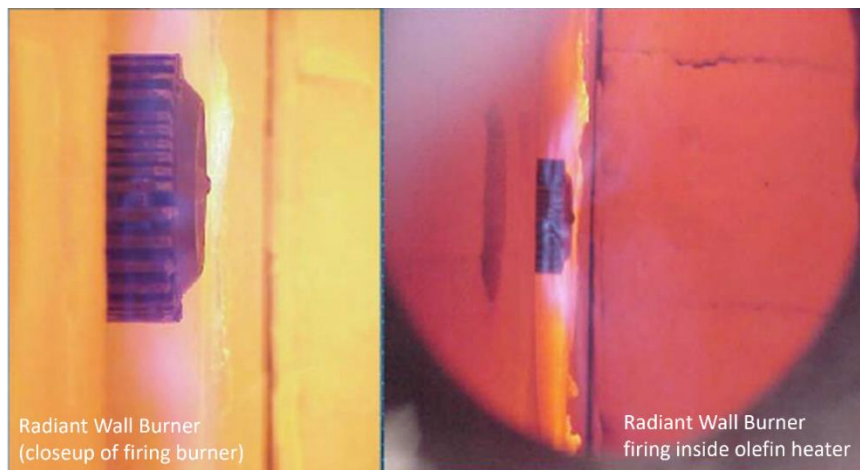


Figure 5 - Radiant wall burner used in Olefin furnace

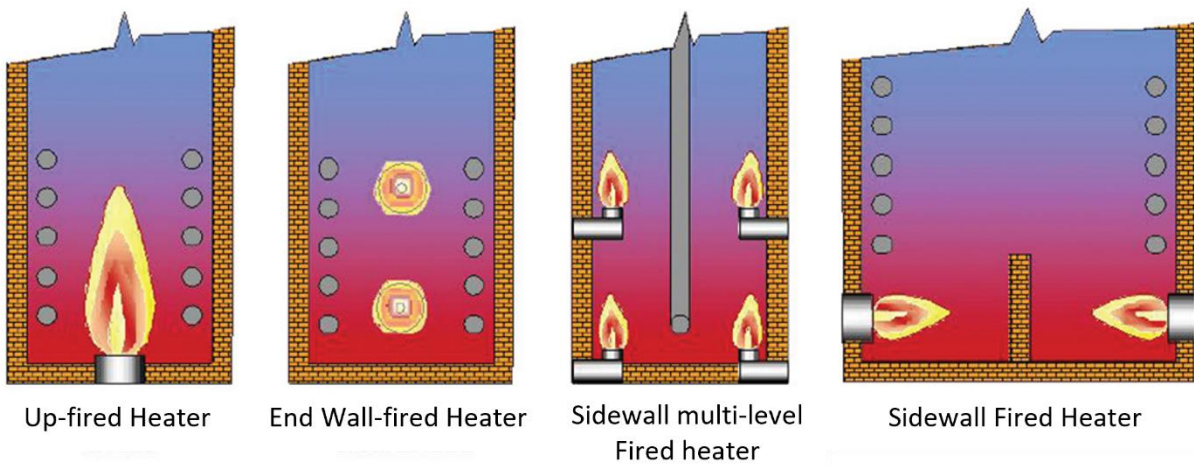


Figure 6 – Furnace/burner configurations for the process industry

Previous combustion testing of hydrogen blending in lab scale and industrial scale burners illustrate the impact of fuel blending. A common hydrocarbon fuel used in the process industry is natural gas (NG). Figure 7 shows flames from a lab-scale burner for varying amounts of hydrogen blended with NG as it increases from 0% (far left) to 100% (far right). Note the change in flame color and flame shape. Similarly, Figure 8 shows flames from an industrial scale burner as the amount of hydrogen blended with propane (C3) is increased from 0% (far left) to 100% (far right). Once again, note the change in flame shape and color. Clearly, hydrogen blending changes the radiation properties of the flame which also impacts process performance which depend on thermal radiation flux from the flames to the heat transfer surface as it does in the petrochemical industry as well as the glass industry and the steel industry.

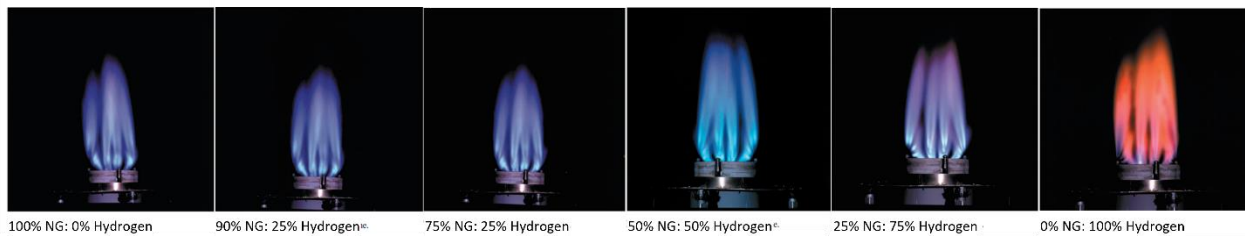


Figure 7 – Hydrogen blended with Natural Gas in a lab-scale burner⁴

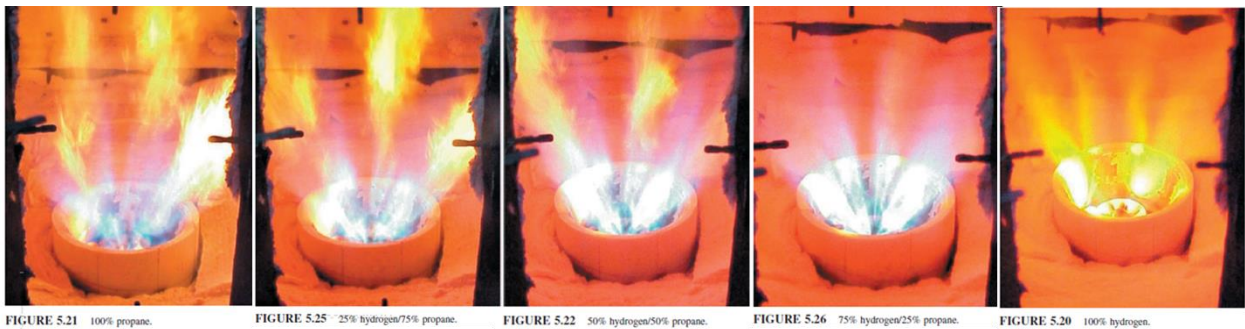


Figure 8 - Hydrogen/Propane flames in an industrial scale burner⁴

Based on the observed impact of blending hydrogen with standard hydrocarbon fuels, the CFD study discussed in this paper is applicable to many industries including steel making, olefin production and others. Given this, the CFD analysis will consider hydrogen blending with NG, LPG and Pressurized NG (LNG). Analysis of the CFD results focused on the impact of hydrogen blending on reducing carbon emissions plus other emissions including NO_x and PM_{2.5}.

⁴ images from Chapter 5, John Zink Combustion Handbook, 2001

METHODOLOGY

To ensure the burner being simulated is operating in a quasi-steady state mode, all transient simulations were run for approximately 10 to 15 seconds of operating time before collecting the final simulation results. This provided a full spectrum of representative flame fluctuations during firing conditions. Since a transient solver is used in this analysis, field variables fluctuate in time due to turbulence and other non-linear effects caused by coupling between the partial differential equations describing conservation of mass, momentum, and energy in the combustion process. Using the procedure described above, “quasi-steady state” operation is confirmed when trends in the predicted variables stop increasing (decreasing) and exhibit random fluctuations associated with turbulent fluctuations in the flow field.

The convergence criteria chosen for all simulations was based on the equation of state being satisfied to within 0.01% at any location in the computational domain. Typically, this convergence criterion is better than the maximum allowable error since the time step constraint is limited by the Courant condition, which allows the flow field to be solved to a higher degree of accuracy.

Due to the relative spatial and temporal scales involved in modeling a multi-fuel burner (see Figure 2), including all geometric details is not practical as it would require an extremely fine computational mesh to properly resolve burner geometric details plus the associated CPU time required to perform a fully transient LES CFD simulation. Instead, this work relied on the previously validated approach to approximate detailed geometry using approximate geometry and source terms that properly captures flow dynamics to predict pressure drop through the actual burner geometry. More critical is the mesh refinement required to accurately simulate jet flow from burner inlet ports. Most multi-fuel burners (see Figure 9) have several inlet ports with port diameter less than 1mm (0.039”).

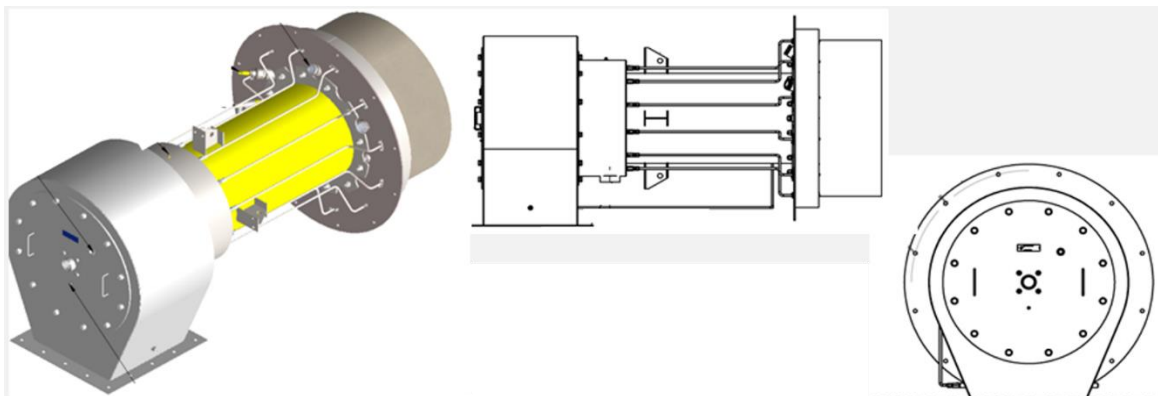


Figure 9 - Multi-port industrial scale burner for firing blended fuels

To simulate the jet flow profile from a single port would require 5 cells in the x and y direction across the port exit and extend at least 10 port diameters beyond the port exit with z-direction cells having a similar size as the x and y-direction cell have which means each port would require a minimum of at least 50 cells above the burner port. Thus, an estimate of the number of cells in the mesh to approximate a burner with 20 ports would be $5 \times 5 \times 50 \times 20 = 25,000$ cells for each burner. A large olefin heater such as shown in Figure 6 which may include 100's of wall burners (Figure 5) and 10's of floor burners (Figure 5 - Radiant wall burner used in Olefin furnace

) would require on the order of at least 1,000,000 computational cells in the near burner regions. Coupled with the number of cells to approximate the entire flow field inside the heater, the total mesh size would easily exceed 100,000,000 cells which would be prohibitive large to conduct meaningful industrial analysis of full-scale industrial systems such as an olefin furnace. *C3d* is tailored to allow fully transient analysis of large burner systems using mass sources located on each burner port. Thus, instead of resolving flow from individual jets coming from each burner port using a refined mesh, *C3d* uses mass sources located on the burner face for each burner port. This approach allows *C3d* to accurately capture individual jet flow dynamics along with coupling between adjacent jets from all burner tips in a full-scale simulation without having to resolve the flow dynamics using a refined mesh.

C3d used a structured grid composed of 583,840 hexahedral cells (see Figure 10) to approximate the burner geometry inside a single burner can. The size of the computational domain was kept small to focus attention on combustion of the blended fuel. In a steady-state RANS CFD analysis, a formal mesh independence study involves halving and doubling cell size in the computational domain. By comparison, *C3d* simulations are transient so mesh independence is checked using several different meshes with varying degrees of refinement near the burner inlets to check for mesh independence. Since the coupled transport processes are complicated by transient non-uniform flow and heat profiles, this approach to mesh independence confirmation has been effective. In *C3d* simulations of burner flames, the code is “tuned” using results from earlier validation cases. This requires that any simulation of a full heater (or other combustion process) would need to use the same base mesh size as the validation case. This criterion establishes the relative cell size and resulting mesh density required for the combustion analysis.

Combustion Model

The LES combustion code *C3d* uses a Smagorinsky-Lilly turbulence model combined with an eddy dissipation approximation of detailed combustion chemistry. The modeling approach involves matching model results with experimental data for a range of cell sizes in the computational mesh with the combustion model tuned for a particular combustion application to model industrial applications of different scales using the same combustion chemistry.

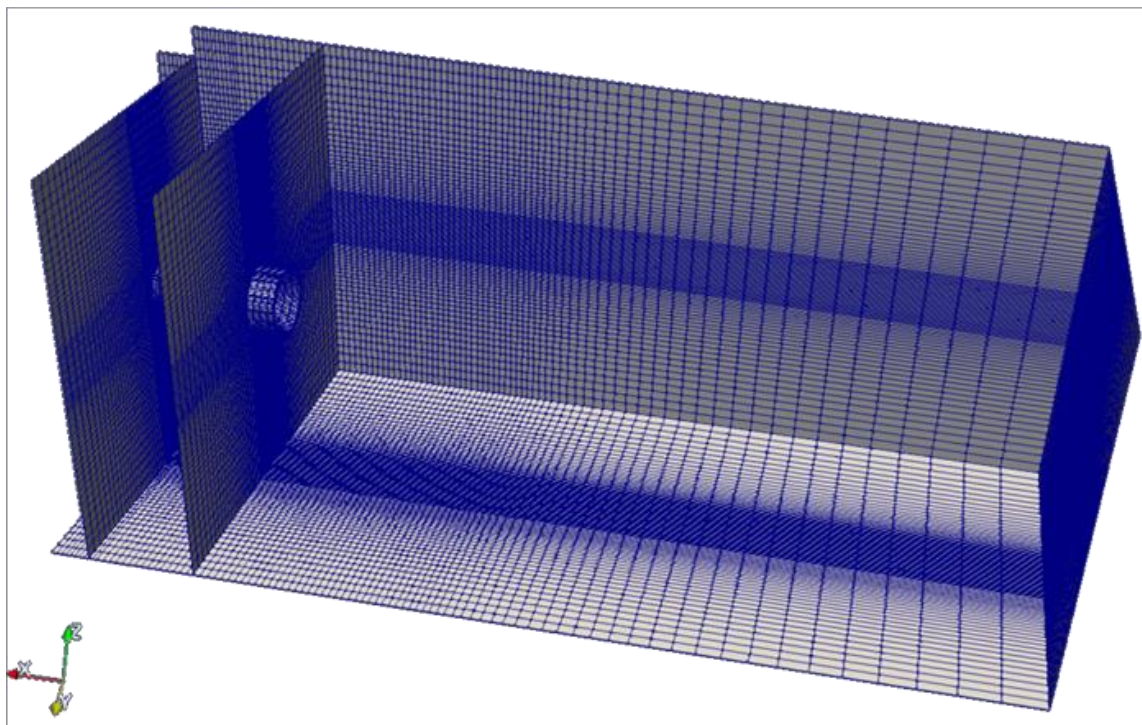


Figure 10 - Computational mesh with 583,840 Hexahedral cells used for blended fuel analysis

Detailed Combustion Chemistry

Often global reaction kinetics are used to model combustion as a single step in CFD simulations. One of the challenges of this approach is applying the reaction mechanism developed from a unique set of test data to set kinetic parameters in the reaction mechanism to other systems. CFD simulation results are sensitive to the mesh cell size, aspect ratio, and number of cells as well as the kinetic data used to build a global combustion model. The combustion model used in this study to model gas burners is discussed below.

To accurately model gas combustion, a consistent set of chemical reactions that describe the overall combustion chemistry is required. To reduce CPU requirements, a subset of chemical reactions from the full set of detailed reactions for methane combustion has been identified.⁵ Based on heat transfer, flame size, and air demand the specific details of the chemical reactions used to model the combustion process are not critical if the oxygen consumption is correctly balanced for a given fuel type and the amount of soot produced is calibrated to match experimental data and observation.

The present combustion analysis of hydrogen/hydrocarbon fuels, a validated combustion model for a wide range of fuels and intermediate species was used.⁶ This model includes primary

⁵ GRI-MECH 3.0 is an example of detailed reaction kinetics that describe methane combustion using 325 reversible reactions containing 53 species (see http://www.me.berkeley.edu/gri_mech/)

⁶ See A. J. Suo-Anttila, "C3d Combustion Model Validation," Albuquerque, January 2019.

fuel breakdown reactions that form intermediate species followed by combustion reactions for those intermediate species. The primary fuel breakdown reactions are shown below for a range of primary hydrocarbon fuels:

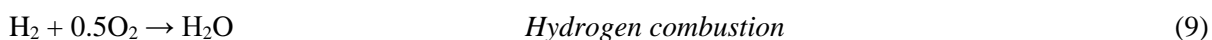


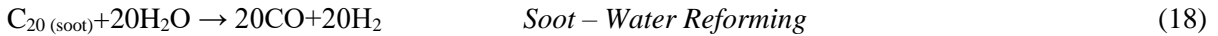
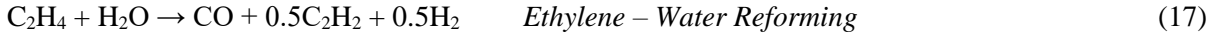
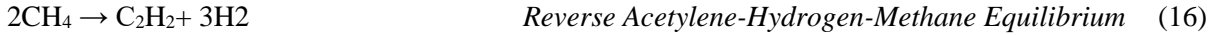
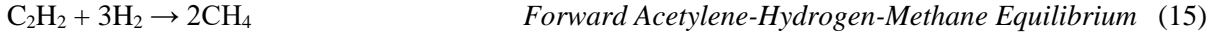
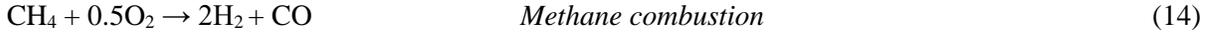
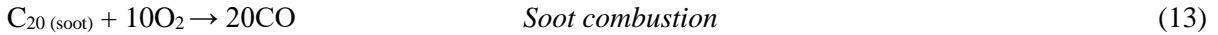
These reactions can be used individually or combined into a single fuel breakdown reaction for a gas mixture by applying the respective mole fractions of each component and adding the mole fraction weighted reactions terms together to form a single fuel breakdown reaction for the mixed fuel. For example, combustion of a gas mixture of ethylene and propylene could be approximated by combining the individual fuel breakdown reactions for ethylene (Eq.1) and propylene (Eq. 7) using the mole fractions of each species in the gas mixture.

For more complex fuels, the mixture could be approximated by breaking down the complex hydrocarbon into CO, C₂H₂, H₂ and H₂O with stoichiometric coefficients estimated using three rules:

- Heavy sooting hydrocarbons produce more C₂H₂ and possibly a small amount of soot,
- The heat release for primary fuel breakdown should be adjusted by producing more H₂O for higher heat release or more H₂ for less heat release, and
- The oxygen consumption balance, and associated CO production should be determined by an elemental balance.

Previous tests of this approach showed that the combustion model based on methane combustion has mild sensitivity to the primary breakdown reactions, which allows flexibility in developing more advanced combustion models for mixed gases. Testing the combustion model in a range of different flame simulations showed that secondary reactions are mostly determined by the flame temperature and soot production.





One advantage of this approach is that the initial reactions for burning the hydrocarbon gas has a low activation energy, which allows partial combustion and heat release from gas combustion. This maintains stable combustion since the partial heat released supports the subsequent combustion reactions, which produce most of the heat and all the soot in the flame.

Similar to previous analysis of flare flames^{7,8} the flare gas Arrhenius combustion time scale is combined with the turbulence eddy breakup time scale to yield an overall time scale for each reaction:

$$t_{total} = t_{arrhenius} + t_{turb} = \frac{1}{C_i} = \frac{1}{A_k T^b \exp\left(-\frac{T_A}{T}\right)} + \frac{C_{eb} \Delta x^2}{\varepsilon_{diff}} \quad (19)$$

where A_k is the pre-exponential coefficient, T_A is an activation temperature, T is the local gas temperature, and b is a global exponent, Δx is the characteristic cell size, C_{eb} is a user input constant (~0.2E-04) that is cell size dependent, ε_{diff} is the eddy diffusivity from the turbulence model, and t_{turb} is the turbulence time scale (characteristic time required to mix contents in computational cell). The reaction rates are combined by simple addition of time scales. Depending on the relative magnitude of the Arrhenius time scale compared to the turbulent time scale, the characteristic time for each reaction may be different. Using this approach, the combustion model approximates turbulent combustion based on the well-known Eddy Dissipation Concept (EDC) and local equivalence ratio effects.

Using this approach, the multi-step chemical reaction model was developed using the breakdown reactions (Eqs. 1-8) and the secondary combustion reactions (Eqs. 9-18) for the blended fuel to be burned in the specific application. All rate equations are solved

⁷ J. Smith, A. Suo-Anttila, S. Smith and J. Modi, "Evaluation of the Air-Demand, Flame Height, and Radiation Load on the Wind Fence of a Low-Profile Flare Using ISIS-3D," *AFRC-JFRC 2007 Joint International Combustion Symposium*, Marriott Waikoloa Beach Resort, Hawaii, October 21-24 (2007).

⁸ J. Smith, A. Suo-Anttila, N. Philpott and S. Smith, "Prediction and Measurement of Multi-Tip Flare Ignition," *American Flame Research Committees - International Pacific Rim Combustion Symposium, Advances in Combustion Technology: Improving the Environment and Energy Efficiency*, Sheraton Maui, Hawaii, September 26-29 (2010).

simultaneously for each reaction and the stoichiometric coefficients are used as constraints to couple the equations and insure conservation of mass (chemical species) and energy.

In the current simulations, the global reaction mechanism described by Suo-Anttila⁶ was used. This work relies on previous work by Duterque *et al.*, 1981⁹ and Kim and Maruts, 2006¹⁰ as starting points. Since the previous work adjusted the global reaction coefficients to match “laminar” flame speed data and since the combustion we are simulating is governed by turbulent mixing, the original coefficients are not directly applicable. Also, since the kinetic coefficients associated with activation temperature and the exponents for mole fractions are based on the physics of the reaction mechanism, they are not affected by local grid structure. However, this was not true for the pre-exponential coefficient. Thus, to match reaction rates with measured combustion rates, the pre-exponential coefficients for all reactions were adjusted to establish a validated combustion model. Also, since the combustion model depends on turbulent mixing of fuel and oxidant, combustion will be governed by turbulent mixing as well. The *C3d* code uses an LES formulation to approximate turbulent mixing, which depends on two additional factors, a proportionality coefficient and the local cell size. The recommended LES proportionality coefficient of 0.15 has been used. To properly capture cell size dependency, the same computational mesh characteristic dimensions were used in the full mesh as used in previous validation studies for the ethylene flame radiation validation test (see Figure 11). Using this information, the required kinetic parameters listed in Table 1 were determined for the validated combustion model used in the present work.

Turbulent Mass Transport and Mixing

C3d is based on a Large Eddy Simulation (LES) formulation to approximate the turbulent combustion. The governing equations for this LES based CFD tool, assuming incompressible fluid flow, as described by Smith, et al., 2017¹¹ are given below by the following equations.

The steady-state continuity equation is:

$$\partial(\rho u_i) / \partial x_j = 0 \quad (20)$$

where ρ is the density of the gas (mixture) and u is the three-dimensional velocity vector.

⁹ J. Duterque, B. Roland and H. T., "Study of Quasi-Global Schemes for Hydrocarbon Combustion," *Combustion Science and Technology*, vol. 26, no. 1-2, pp. 1-15, 1981.

¹⁰ I. Kim and K. Maruts, "A Numerical Study on Propagation of Premix Flames in Small Tubes," *Combustion and Flame*, vol. 146, pp. 283-301, 2006.

¹¹ J. Smith, B. Adams, R. Jackson and A. Suo-Anttila, "Use of RANS and LES Turbulence Models in CFD Predictions for Industrial Gas-fired Combustion Applications," *Journal of the International Flame Research Foundation*, Article number 201607, ISSN 2075-3071 (December 2017);

<http://www.industrial.combustion.ifrf.net/papers.html>



Figure 11 – Comparison of Predicted and Measured Flame Shape for an ethylene combustion test (predicted flame image overlaid to measured flame image)

Table 1 - Reaction parameters used in MPGF combustion model

Reaction	f_1	f_2	T_A (K)	C (1/s)	B
Primary Fuel Breakdown (ethylene)	$[C_2H_4]^{0.1}$	$[O_2]^{1.65}$	0 K	1	2
Hydrogen Combustion	$[H_2]^{0.33}$	O_2	10000 K	1e8	0
Acetylene combustion & soot nucleation	$[C_2H_2]^{0.33}$	O_2	15110 K	2e8	2
Acetylene + soot growth	$[C_{20}]^{0.33}$	C_2H_2	15110 K	1e7	0
CO – Oxygen combustion	CO	$[O_2]^{0.25}[H_2O]^{0.5}$	20142 K	1e18	0
Soot combustion	$[C_{20}]^{0.33}$	O_2	0 K	0.5	0.75
Methane combustion	CH_4	O_2	15000 K	1e12	0
Forward Acetylene – Hydrogen – Methane	C_2H_2	H_2	15110 K	5e7	0
Reverse Acetylene – Hydrogen - Methane	CH_4	CH_4	23500 K	4e9	0
Ethylene - Water Reforming	C_2H_4	H_2O	15000 K	5e6	0
Soot – Water Reforming	$[C_{20}]^{0.1}$	$[H_2O]^{1.7}$	0 K	1.0	0.75

The momentum equation is:

$$\partial(\rho u_i u_i) / \partial x_j = \partial P / \partial x_i + \partial \tau_{ij} / \partial x_j + \rho f_i \quad (21)$$

with f_i as the body forces, P as the pressure, and τ_{ij} represented as the stress defined as:

$$\tau_{ij} = \mu(\partial u_i / \partial x_j + \partial u_j / \partial x_i) + (\mu_B - 2/3 \mu) \partial u_k / \partial x_k \delta_{ij} \quad (22)$$

The other governing equation solved in C3d is the energy equation:

$$\rho c_p \partial (T) / \partial x_j = -(\nabla \cdot q) - \left(\frac{\partial \ln \rho}{\partial \ln T} \right) \frac{Dp}{Dt} - (\tau : \nabla v) \quad (23)$$

where C_p is the specific heat. The energy equation is used to capture the temperature changes due to combustion and mixing. The energy equation also includes radiation effects.

To resolve the sub-filter scales for the LES turbulence model, a Gaussian filter is used:

$$G(x - r) = \left[\frac{6}{(\pi \Delta^2)} \right]^{(1/2)} \exp \left(-\frac{6(x - r)^2}{\Delta^2} \right) \quad (24)$$

The following equations are used to simulate the kinetic energy dissipation on subgrid scales to molecular diffusion:

$$\tau_{ij}^r - 1/3 \tau_{kk} \delta_{ij} = -2\nu_t \bar{S}_{ij} \quad (25)$$

$$\bar{S}_{ij} = 1/2 \left(\frac{\partial \bar{u}_i}{\partial x_j} + \frac{\partial \bar{u}_j}{\partial x_i} \right) \quad (26)$$

with τ_{ij}^r as the stress tensor, \bar{S}_{ij} as the rate-of-strain tensor, and ν_t as the turbulent eddy viscosity. The eddy viscosity is approximated as the characteristic length scale times the velocity scale in the subgrid scale model as implemented in the Smagorinsky-Lilly model:

$$\nu_t = (C_s \Delta_g)^2 \sqrt{2 \bar{S}_{ij} \bar{S}_{ij}} = ((C_s \Delta_g)^2 |S|), \quad C_s = \text{Constant}, \quad \Delta_g = \text{grid size}$$

The equilibrium assumption was applied between energy production and dissipation of small scales in this model. The multi species conversation equations form is shown in equation (14)

$$\frac{\partial \rho m_i}{\partial t} + \nabla \cdot \rho V m_i = -\nabla \cdot \vec{J}_i + R_i + S_i \quad (27)$$

where, m_i is the mass fraction of species i , \vec{J}_i is the diffusion flux of species i , R_i is the mass creation or depletion by chemical reactions, and S_i mass source. The species equations are solved to keep track of the distribution and concentration of fuel, oxygen, intermediate species, soot, and products of combustion (CO_2 and H_2O). The combustion model was used to provide the species equations source and sink terms as a function of species concentrations, local gas temperature, and turbulent diffusivity.

Flame Radiation

C3d includes sub-models to predict flame emissivity as a function of molecular gas composition, soot volume fraction, flame size, shape, and temperature distribution which in turn depend on solutions to the mass, momentum, energy, and species transport equations. The radiation transport model predicts radiation flux on external (and internal) surfaces and also provides source and sink terms to the energy transport equation to ensure an accurate prediction of flame temperature distribution.

Thermal radiation effects in *C3d* are calculated in two ways. Within the flame zone, radiation is assumed to be diffusive and outside the flame zone radiative transport is calculated using view-factor methods. The flame surface used in the view-factor calculation is set by finding the dynamic surface wherein a product of hydrocarbon combustion, typically carbon dioxide, has a mass fraction above and below a user specified value, typically 0.04. This dynamic surface, its temperature, and a correction factor (dependent upon flame optical thickness) are all used to calculate view-factor radiation from all flame surfaces to surrounding objects including nearby process instruments, equipment, and structures to identify safe work zones. The view-factor radiation calculation also includes shadowing due to intervening objects. It also includes radiation absorption along the ray path due to participating media including water vapor, carbon dioxide, and soot. Finally, it includes absorption and re-radiation from the ground.

The view-factor radiation calculation has also been implemented in a multi-zone version of *C3d* to allow multi-block meshes required for large systems including simulations of full combustion systems (i.e., multi-burner configurations shown in Figure 6). The multi-block formulation allows a user to split a large problem into separate zones coupled together at the boundary conditions. The full equation set for a specific zone is solved on a different CPU with time synchronized so large problems requiring 10's to 100's of millions of cells can be solved on multiple CPU's simultaneously to reduce overall computational time. The view-factor thermal radiation from one block (or zone) can be calculated to any geometric position either within or outside that zone. This allows the user to add radiation contributions from adjacent zones to get the total incident radiation value for the entire problem. The only restriction in this zone-to-zone radiation transport method is related to shadowing and media absorption in adjacent zones that is not considered because adjacent zones only have information about geometric and compositional details within the specific zone boundary.

Boundary Conditions

General boundary conditions considered in *C3d* include an imposed flow profile on one side of a domain with hydrostatic pressure boundaries on all other sides except the floor where a zero mass-flux boundary is imposed. Thermal and species boundary conditions are set for specific firing conditions assuming the entrained fluid composition and temperature. Boundary conditions for specific burner tips are set using a 1-D grid connected to a point source in the domain. This approach allows use of individual ports in a single burner or use of multiple burners in a domain. This allows *C3d* to simulate large multi-burner systems as discussed earlier with each burner having several individual ports. This approach also facilitates matching the flow profile exactly without using greatly refined mesh around each burner which greatly simplifies the calculation and significantly reduces required CPU time.

Modeling Assumptions

Based on the methodology discussion just given, the following assumptions are used when modeling an MPGF flare:

1. Combustion of the flare gas is approximated by the chemical reaction mechanism described above using specified kinetics (see Table 1).
2. Jet flow from burners is approximated using mass sources specified on burner faces.
3. Thermal radiation is calculated using the standard radiation model included in *C3d*.
4. Mesh refinement is sufficient to provide mesh independent results.
5. Hydrostatic boundary conditions allow flow in and out of the boundaries for large multi-zone approximation of full furnace simulations.

Code Validation

Predicting heat transfer from the flare flame depends on accurate simulation of the combustion chemistry that controls flame size and shape together with how heat is transferred from the flame to its surroundings. Most energy from a burner flame is carried away by convective flow associated with the heated plume coming from the flame. However, a fraction of the total energy from the flame leaves the flame via thermal radiation. The radiation model used in *C3d*, discussed elsewhere¹², has been validated by comparing predicted radiation heat loss from the flame created by a multi-burner system to predicted values from *C3d*.

Radiation validation studies were performed for propylene fuel fired through a single burner tip with 5,465 kg/sec propylene injected at 22.5 PSIG. During this validation test, the burner was fired with a crosswind blowing 3 - 7mph (gusting to 9-13mph). Radiation flux was measured at 75 ft, 100 ft, and 150 ft distance from the flame and at 5 ft and 20 ft elevation from the ground. Radiometers were located due east of the flame with the crosswind blowing from the SSE 169 degrees from true north.

Simulations were performed considering a 5mph and a 10mph crosswind. Previous work has shown that flame radiation is sensitive to crosswind speed. Validation simulations included radiation attenuation due to CO₂ and H₂O absorption using the Fuss and Hamins correlation.¹³

The *C3d* simulation included a 12m x 12m x 20m (40ft x 40ft x 65ft) computational domain using variable mesh spacing of 328,000 cells. A comparison between measured radiation results and predicted radiation results are shown in Table 2. Measured results are within predicted results from the two bracketing wind speeds considered. This work reaffirmed earlier observations that flame radiation is very sensitive to crosswind speed.

Figure 12 shows the variation of flame temperature with equivalence ratio for hydrogen air mixtures, hydrogen fuel blends and laminar flame speeds for different fuel air mixtures.

¹² J. Smith, R. Jackson, A. Suo-Anttila, K. Hefley, Z. Smith, D. Wade, D. Allen and S. Smith, "Radiation Effects on Surrounding Structures from Multi-Point Ground Flares," *AFRC Industrial Combustion Symposium*, Historic Fort Douglas Officers Club University of Utah, Salt Lake City, Utah (September 9-11, 2015).

¹³ S. Fuss and A. Hamins, "An estimate of the correction applied to radiant flame measurements due to attenuation by atmospheric CO₂ and H₂O," *Fire Safety Journal*, vol. 37, pp. 181-190 (2002).

Table 2 - Comparison of predicted and measured radiation fluxes at 6 locations for 2 wind speeds

Elevation (wind speed)	5 ft high (3-7mph measured wind)	5 ft high (5mph predicted wind)	5 ft high (10mph predicted wind)	20 ft high (3-7mph measured wind)	20 ft high (5mph predicted wind)	20 ft high (10mph predicted wind)
Radiometer distance from flare	Measured Flux (BTU/hr-ft ²)	Predicted Flux (BTU/hr-ft ²)	Predicted Flux (BTU/hr-ft ²)	Measured Flux (BTU/hr-ft ²)	Predicted Flux (BTU/hr-ft ²)	Predicted Flux (BTU/hr-ft ²)
75 feet	171	190	168	205	221	183
100 feet	102	117	95	102	120	104
150 feet	34	53	38	34	53	38

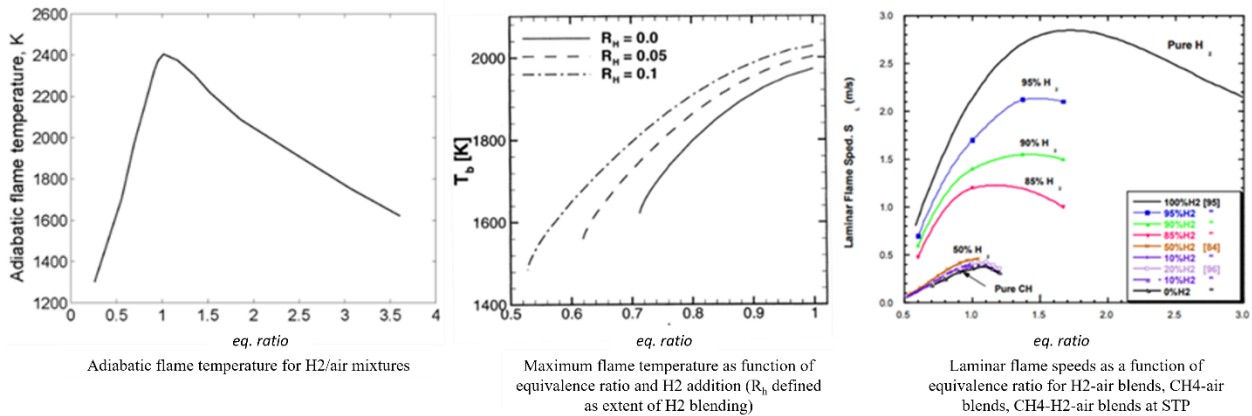


Figure 12. Variation of flame temperature with equivalence ratio, for different fuels and for different H₂ blends.¹⁴

COMBUSTION ANALYSIS OF HYDROGEN BLENDED FUELS

Typical composition of natural gas includes a mixture of light hydrocarbons mostly methane (C1), ethane (C2), propane (C3), butanes (C4), and pentanes (C5). FG composition varies by source as shown in Table 3.

Combustion tests have been performed using blended fuels illustrate the impact H₂ has on the flame shape and color. Experiments conducted in the lab using lab-scale burners (Figure 7) and in industrial testing using industrial-scale burners (Figure 8) demonstrate the impact hydrogen blending with standard hydrocarbon fuels have. Scheler et al., 2007¹⁴ also discusses the impact fuel blending has on burner performance in terms of how equivalence ration impacts flame temperature and laminar flame speed (see Figure 12). As shown above, hydrogen blending impacts flame temperature with the maximum flame temperature occurring when the fuel/air mixtures are slightly rich (see Figure 13).

¹⁴ Scheler, R.W., White, C. and Keller, J., “Chapter 8 – Lean Hydrogen Combustion,” SAND2007-1524P, Sandia National Laboratory, Livermore, CA (2007)

Table 3 – Composition of Commercial Natural Gas by location¹⁵

Fuel Gas Component	Sample Gas Compositions by Production Region (vol%)										
	Tulsa, OK	Alaska	Algeria	Netherlands	Kuwait	Libya	North Sea	Alabama	Ohio	Missouri	Pennsylvania
CH ₄	93%	100%	87%	81%	87%	70%	94%	90%	94%	84%	83%
C ₂ H ₆	3%	—	9%	3%	9%	15%	3%	5%	3%	7%	16%
C ₃ H ₈	1%	—	3%	<1%	2%	10%	1%	—	<1%	—	—
C ₄ H ₁₀	<1%	—	1%	<1%	1%	4%	<1%	—	<1%	—	—
C ₅ & higher	—	—	—	—	—	—	—	—	—	—	—
CO ₂	1%	—	—	1%	2%	—	<1%	—	1%	1%	—
N ₂	2%	1%	<1%	14%	1%	1%	2%	5%	1%	8%	1%
O ₂	—	—	—	—	—	—	—	—	<1%	—	—
H ₂	—	—	—	—	—	—	—	—	<1%	—	—
Total	100%	100%	100%	100%	100%	100%	100%	100%	100%	100%	100%

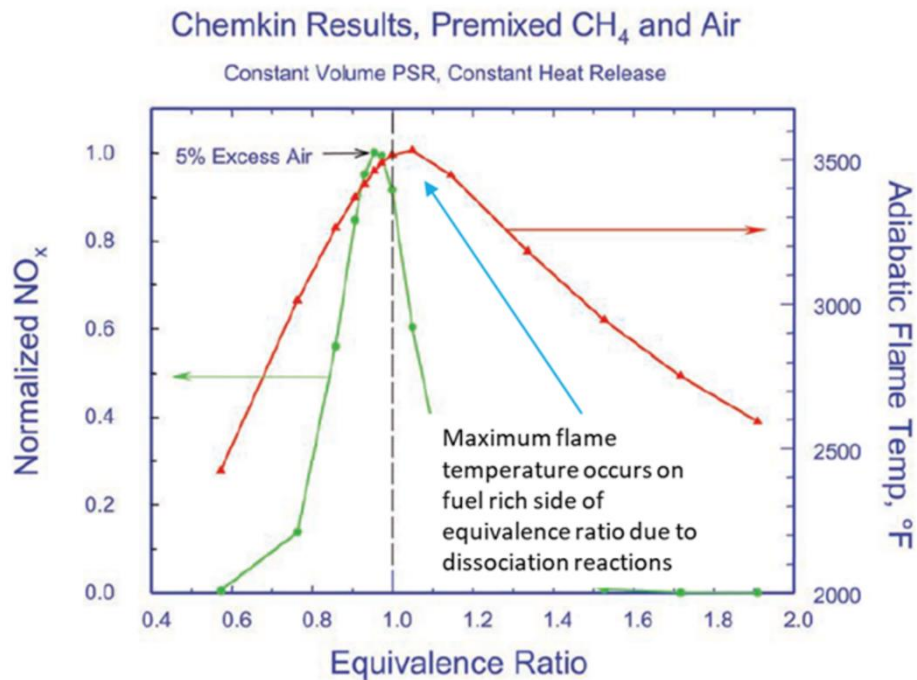


Figure 13 - Variation of peak temperature with equivalence ratio for NG/air flames

Using the validated CFD code, *C3d*, a detailed analysis has been completed for blended NG/H₂ and LPG/H₂ cases with blends ranging from 0% to 100% hydrogen. Results from each case have been quantified comparing combustion temperature, flame shape/flame size, and NO_x and CO₂ emissions.

Process Conditions

Process conditions for the 100% natural gas (0% hydrogen) case are given below:

¹⁵ Adapted from Reed, R.J., North American Combustion Handbook, Vol. 1., North American Mfg. Co., Cleveland, OH (1986)

Table 4 - Process Conditions for CFD cases

Fuel Flow Rate (kg/s)	0.47
Combustion Air Flow Rate (kg/s)	18.45 (124.9% excess air)
Heat Release Rate of Fuel (MW)	23.45

Starting with the 0% hydrogen case, the heat release rate and combustion air flow rate were maintained the same for all subsequent blended fuel cases (20%, 40%, 60%, 80% and 100% hydrogen by volume). The same process conditions were used for Natural Gas (NG) cases and the Liquefied Petroleum Gas (LPG) cases for varying amounts of hydrogen blend (0%, 20%, 40%, 60%, 80% and 100% by volume) while maintaining the heat release rate from the fuel of 23.45 MW with a constant flowrate of combustion air (18.45 kg/s). LPG typically contains a mixture of propane, propylene, butylene, isobutane, and n-butane. LPG is used in heating appliances, cooking equipment, and vehicles. When used as a vehicle fuel, it is sometimes referred to as “Autogas” or just Gas. In the US, the composition of LPG is typically 100% propane which is the composition used in these cases. The process conditions for the 100% LPG case (0% hydrogen) are summarized in Table 5.

Table 5 - Process Conditions for 100% LPG case

Fuel Flow Rate (kg/s)	0.51
Combustion Air Flow Rate (kg/s)	18.45 (128.9% excess air)
Heat Release Rate of Fuel (MW)	23.45

Note that the fuel flow rate is different than that shown in Table 4. For all cases, the heat release from the fuel was kept constant so as the degree of H₂ blending changed the hydrocarbon fuel flow was changed to keep the heat release constant and the amount of excess air was changed to keep the equivalence ration constant. With this basis, CFD cases were run for NG blended with hydrogen and LPG blended with hydrogen considering 0% H₂, 20% H₂, 40% H₂, 60% H₂, 80% H₂ and 100% H₂ (six cases for each hydrocarbon fuel). Results of each of these cases are compared by the predicted flame shape and centerline temperature profile. A summary table is also provided to compare results from each blended fuel analysis.

Natural Gas/Hydrogen Blended Fuel Cases

The predicted flame shape and size for NG/H₂ blended cases are shown in Figure 14. These flame shapes are shown using CO iso-surfaces colored by temperature. As expected, flame temperature is relatively cooler for NG rich flames compared to those with higher H₂ blends. Flame shape appears more diffuse for NG rich flames compared to H₂ rich flames.

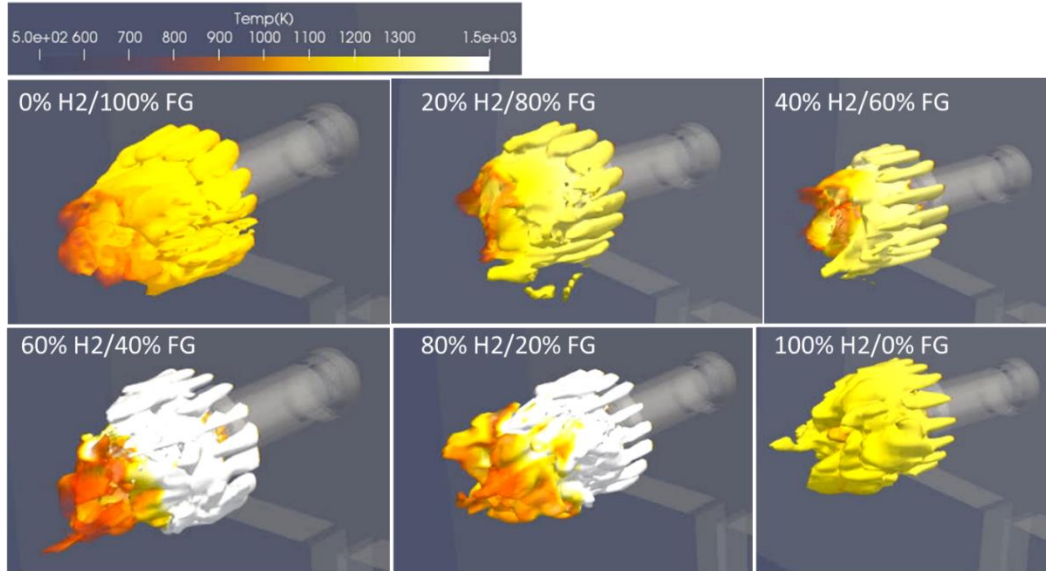


Figure 14 - Natural gas and hydrogen blended flames

A comparison of centerline temperature profile for all NG/H2 cases are shown in Figure 15. As shown above, flame shape appears bushier for NG rich flames compared to H2 rich flames.

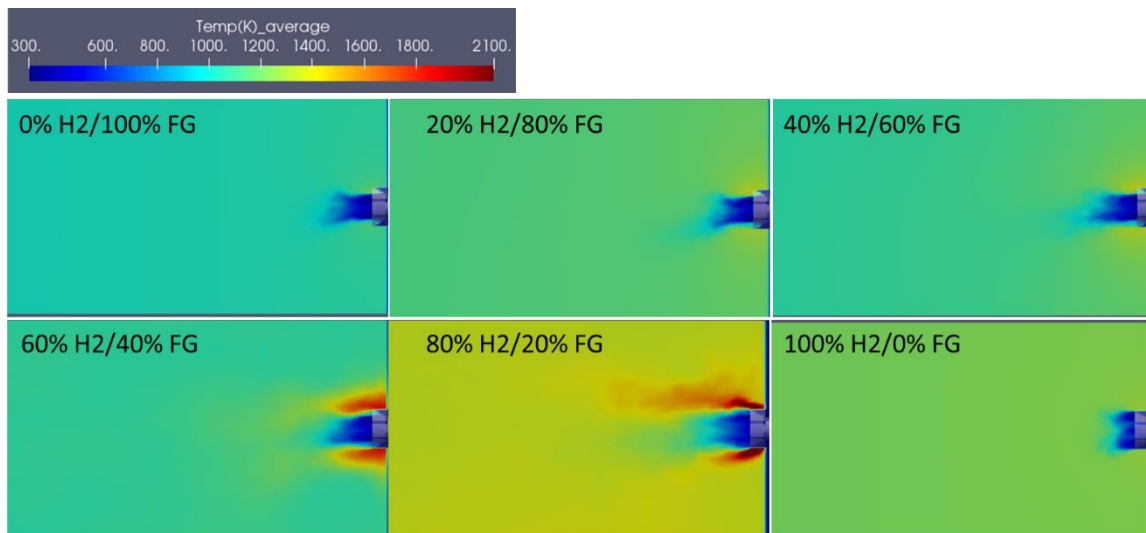


Figure 15 – Predicted temperatures for NG/H2 flames – results time averaged over 5 seconds

CFD results for all NG/H2 cases are shown in see Table 6. As shown, combustion temperature reaches a maximum for the 80% H2 case. Excess changes to maintain equivalence ratio which impacts the maximum combustion temperature and the predicted exit temperature.

Table 6 - Comparison of NG/H2 blended fuel cases (species concentration given on mass frac basis)

NG+H2	Excess Air (%)	Max Temp (K)	Exit Temp (K)	Exit O2	Exit CO	Exit CH4	Exit CO2	Exit H2O
0% H2	124.86%	1303	1030	0.107	1.00E-08	9.60E-09	0.069	0.095
20% H2	127.53%	1330	968	0.1	1.00E-08	9.50E-09	0.066	0.104
40% H2	131.26%	1630	1210	0.084	1.00E-08	9.50E-09	0.046	0.132
60% H2	137.10%	1590	1217	0.083	1.00E-08	9.60E-09	0.047	0.133
80% H2	147.20%	1628	1233	0.085	1.00E-08	9.60E-09	0.046	0.132
100% H2	168.99%	1170	1106	0.128	0.00E+00	0.00E+00	0.004	0.119

Due to the large residence time in the burner can, there is very little predicted difference for pure natural gas to pure hydrogen in terms of outlet CO and CH4 mass fractions which indicates complete combustion for all cases. Considering the adjusted fuel mass flow for each case with the increased air flow to maintain a constant heat release for each case, there is a 3% reduction in predicted CO2 at the exit between the 0% H2 and 40% H2 cases. Also, there is a 10% reduction in predicted CO2 level between the 0% H2 and 60% H2 cases. Finally, there is a 32% reduction in predicted CO2 level between the 0% H2 and 80% H2 cases. This indicates the most effective fuel blend for NG in terms of reduction in CO2 emission is 80% H2.

LPG/Hydrogen Blended Fuel Cases

The predicted flame shape and size for the LPG/H2 blended fuel cases are shown in Figure 16. For these cases, the flames show relatively cooler temperatures for the LPG rich flames with the flame temperature increasing with the amount of hydrogen blend. Flames with lower hydrogen appear bushier than high hydrogen flames.

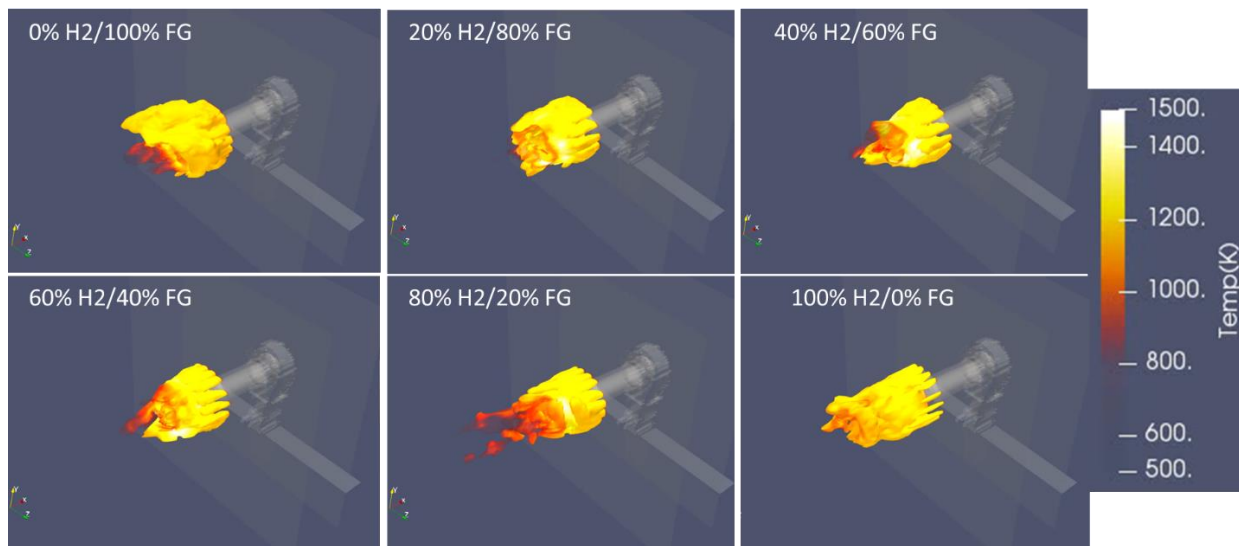


Figure 16 - LPG and hydrogen blending flame envelope comparison

A comparison of the predicted temperature profiles on a centerline plane for all LPG/H₂ cases is shown in Figure 17. This image confirms the observation that flames with higher hydrogen are more defined (less bushy) than flames with lower hydrogen blends.

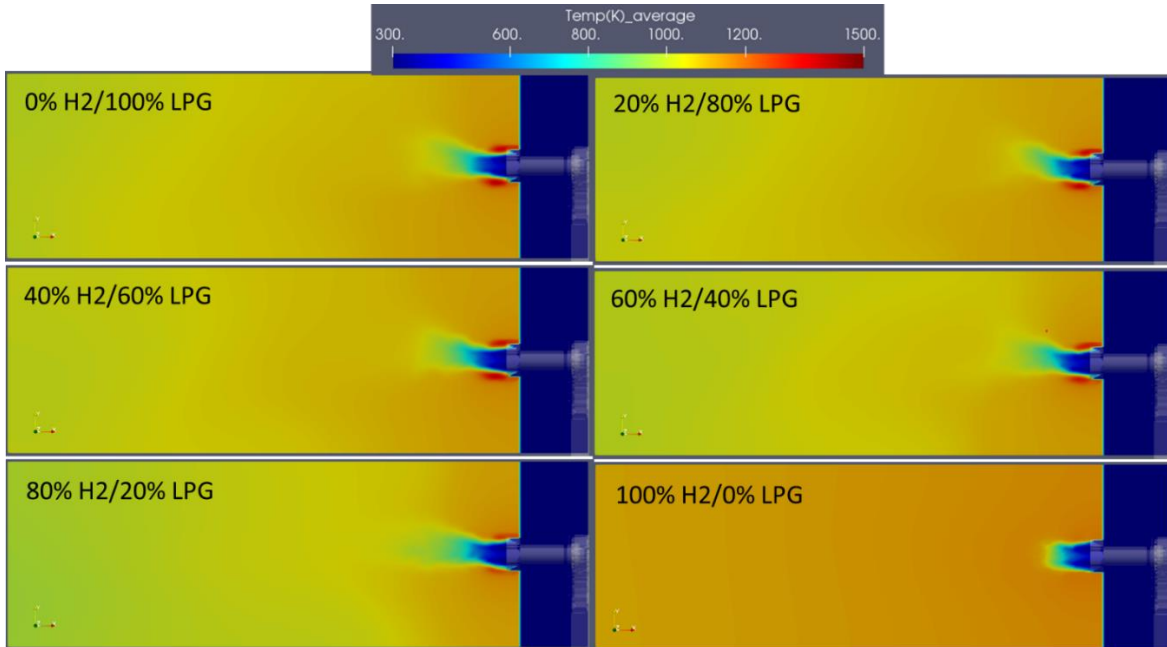


Figure 17 - LPG and hydrogen blending temperature profile comparison

A summary of the predicted metrics for the LPG/H₂ blended cases is given in Table 7. As before, the excess air has been changed to maintain the equivalence ratio for all cases. As observed earlier, exit temperatures for lower hydrogen blended cases are lower than those for the higher hydrogen blended cases (1002K for 0% H₂ vs 1106K for 100% H₂). Unlike the NG/H₂ blended cases, the exit temperature reaches a minimum for 80% H₂ blend. For these cases, predicted NO_x levels at the exit are included. As expected, for hotter flames, exit NO_x levels increase.

Table 7 - Comparison of LPG/H₂ blended fuel combustion (species values given on mass fraction basis)

LPG+H ₂	Excess Air (%)	Max. Temp. (K)	Exit Temp. (K)	Exit O ₂	Exit CO	Exit C ₃ H ₈	Exit CO ₂	Exit H ₂ O	Exit NO _x (ppm)
0% H ₂	128.90%	1424	1002	0.116	8.70E-09	9.20E-09	0.091	0.069	51
20% H ₂	129.87%	1378	1008	0.117	8.60E-09	9.30E-09	0.09	0.07	49
40% H ₂	131.40%	1394	1012	0.114	8.60E-09	9.30E-09	0.088	0.073	53
60% H ₂	134.13%	1339	1013	0.114	8.70E-09	9.20E-09	0.082	0.076	54
80% H ₂	140.35%	1267	967	0.114	8.60E-09	9.30E-09	0.069	0.085	66
100% H ₂	168.99%	1170	1106	0.128	0.00E+00	0.00E+00	0.004	0.119	67

The summary of the results presented in the last few figures and tables indicates the effect that blended fuel composition has on flame radiation to the vessel walls. It is well known that both NG/H₂ blends produce negligible soot (no soot for 100% hydrogen), so flame temperature and flame surface area have a greater influence on radiation flux to the walls than in a case with radiating soot particles as is the case for combustion of heavy hydrocarbons. This implies burner design to maximize thermal radiation from the flame is important.

SUMMARY AND CONCLUSIONS

In summary, the following points can be drawn from this work:

- Incorporating hydrogen blending with hydrocarbon fuels may be safer and less prone to operational issues in diffusion type burners compared to premixed or partially premixed burners due to hydrogen's higher flame speed compared to hydrocarbon fuels.
- Using hydrogen blended fuels reduces carbon dioxide emissions which may reduce the need for carbon capture equipment which may reduce the capital expenses required to meet increasing regulations related to greenhouse emissions.
- The potential for using hydrogen blended fuels may be dictated in part by the industrial application itself.
- Hydrogen's higher adiabatic flame temperature compared to other hydrocarbon fuels may increase thermal NO_x production. However, keeping the heat release constant by adjusting fuel flow rate and adjusting the air flow rate to maintain equivalence ratio has been shown to maintain NO_x production levels for blended fuels.
- Radiative heat transfer in hydrogen blended fuel combustion is increased due to higher flame temperatures but reduced because of less soot radiation. This effect is fuel dependent given different sooting tendency of heavier hydrocarbon fuels. The result is mainly manifest in changing radiation flux profile to heat transfer surfaces in the specific application.

Based on this work, the following can be concluded related to hydrogen blending with hydrocarbon fuels:

- As hydrogen fed to the burner increases, mixing between fuel and air changes. Hydrogen diffusion into the air stream burns hydrogen near burner inlets.
- Combustion is delayed since the O₂ is consumed by hydrogen early in the combustion process resulting in it being unavailable to burn secondary fuel.
- High temperature hydrogen flames near the burner face increases radiation flux to burner face which results in increased surface temperatures which may lead to increased thermal fatigue and premature failure. This might be alleviated by judicious use of excess air or use of steam injection.
- Adding hydrogen decreases CO and CO₂ levels in the combustion chamber until all carbon emissions are completely eliminated during 100% hydrogen operation.

- Water formed near the burner face during combustion of high hydrogen blended fuels may lead to surface corrosion in the burner if air flow to burner face does not push water vapor away from the burner face into the combustion zone.
- Cases with higher hydrogen blending will require increased levels of excess air to support increased fuel flow needed to maintain a constant heat release rate. However, increased air and higher flame temperature counterbalance each other in terms of overall combustion temperature.

The main conclusion which is clearly the motivation for hydrogen blending in combustion processes used in the metals industry is that by adding hydrogen to hydrocarbon fuels when combustion is required and used to generate process heat needed in specific applications does reduce carbon emissions from them metal industry. This last conclusion is critical in a “carbon constrained” environment for the steel industry.